

Variation on the Kolmogorov Forcing: Asymptotic Dissipation Rate Driven by Harmonic Forcing

B. ROLLIN¹†, Y. DUBIEF¹ AND C.R. DOERING²

¹School of Engineering, University of Vermont, Burlington, VT 05405, USA

²Department of Mathematics, University of Michigan, Ann Arbor, MI 48109-1109, USA

(Received ?? and in revised form ??)

The relation between the shape of the force driving a turbulent flow and the upper bound on the dimensionless dissipation factor β is presented. We are interested in non-trivial (more than two wave numbers) forcing functions in a three dimensional domain periodic in all directions. A comparative analysis between results given by the optimization problem and the results of Direct Numerical Simulations is performed. We report that the bound on the dissipation factor in the case of infinite Reynolds numbers have the same qualitative behavior as for the dissipation factor at finite Reynolds number. As predicted by the analysis, the dissipation factor depends strongly on the force shape. However, the optimization problem does not predict accurately the quantitative behavior. We complete our study by analyzing the mean flow profile in relation to the Stokes flow profile and the optimal multiplier profile shape for different force-shapes. We observe that in our 3D-periodic domain, the mean velocity profile and the Stokes flow profile reproduce all the characteristic features of the force-shape. The optimal multiplier proves to be linked to the intensity of the wave numbers of the forcing function.

1. Introduction

In the first half of the twentieth century, authors such as Richardson (1922), Taylor (1938) and Kolmogorov (1941) developed a description of turbulence based on the concept of an energy cascade. In this defining description of the turbulence phenomenon, kinetic energy is transferred at a constant rate from larger unstable eddies to smaller eddies. The cascade lasts until the eddy motion becomes stable and viscosity can effectively dissipate the kinetic energy. The rate of dissipation of kinetic energy ε is defined by:

$$\varepsilon = 2\nu \langle S_{ij} S_{ij} \rangle \quad (1.1)$$

where S_{ij} is the rate of strain tensor and ν the kinematic viscosity coefficient. Analyses of the Navier-Stokes equations show that bounds on the kinetic energy dissipation rate can be derived directly from these governing equations without additional hypothesis or approximations for statistically stationary incompressible flows. During the 1990s, rigorous bounds for different types of boundary driven flows were derived in the asymptotic case of an infinite Reynolds number Re (Doering & Constantin 1992; Marchioro 1994; Wang 1997):

$$Re = Ul/\nu, \quad (1.2)$$

† To whom correspondence should be addressed

where $U = \sqrt{\langle \mathbf{u}^2 \rangle}$ is the steady-state root mean square value of the total velocity field and l a characteristic length scale of the flow. Variational methods for optimizing the values of the bounds were later introduced by Doering & Constantin (1994) and Constantin & Doering (1995). Since then, these methods have been at the center of the quantitative evaluation of the upper bounds on the dissipation rate in boundary-driven turbulent flows (Nicodemus *et al.* 1998; Kerswell 1998). The first rigorous limits on bulk dissipation for body-force-driven turbulence in a fully periodic domain were derived by Childress *et al.* (2001) and Doering & Foias (2002). Their result indicates that for the three-dimensional Navier-Stokes equations, the energy dissipation rate ε satisfies:

$$\varepsilon \leq c_1 \nu (U^2/l^2) + c_2 (U^3/l), \quad (1.3)$$

where l is the longest characteristic length scale in the body-force function and c_1 and c_2 are coefficients that depend only on the functional shape (defined more precisely in the next section) of the body-force. Dividing equation 1.3 by U^3/l yields:

$$\beta \leq c_1 \frac{1}{Re} + c_2, \quad (1.4)$$

where $\beta = \varepsilon l / U^3$ is the dimensionless dissipation factor. The behavior of the dissipation factor implied by this relation is in qualitative agreement with theoretical, computational and experimental results for homogeneous isotropic turbulence (Frisch 1995; Sreenivasan 1984, 1998). Doering *et al.* (2003) derived an explicit upper bound for β depending only on the shape of the external forcing at high Reynolds number. The perspective of determining a value for ε , via β , directly from the external forcing function presents invaluable advantage since nearly all current turbulent models rely on the prediction of ε from a solution of a transport equation or semi-empirical models.

In this short paper, we present the results of a systematic study of the qualitative features of the bounds on the dissipation factor. Few comparisons have been made between the bounds obtained through analytical derivations and the results given by Direct Numerical Simulations (DNS). Moreover, only canonical large scale forcing such as Kolmogorov flow (Childress *et al.* 2001) or constant shear (Doering *et al.* 2003) has been tested. Using non-trivial forcing functions, we focus, first, on the extent of the β dependence on the body-force-shape. Second, we analyze the mean profile dependence on the force profile.

2. Bound on the dissipation factor

2.1. Definitions

We are considering a body-force driven incompressible flow on a minimal domain (Jiménez & Moin 1991) periodic in three directions. The dynamics of the flow is governed by the Navier-Stokes equations for an incompressible fluid:

$$\frac{\partial \mathbf{u}}{\partial t} + (\mathbf{u} \cdot \nabla) \mathbf{u} + \nabla p = \nu \nabla^2 \mathbf{u} + \mathbf{f} \quad (2.1)$$

$$\nabla \cdot \mathbf{u} = 0, \quad (2.2)$$

where \mathbf{u} is the velocity vector, p is the pressure and \mathbf{f} the driving force. The derivation of the bound on the dissipation factor β in our case is identical to the one made by Doering *et al.* (2003) for the case of a body-forced plane shear flow, except for the boundary conditions. We therefore limit ourselves to recalling the key points of that derivation and refer to their work for the detailed description of the solution of the variational problem.

The steady force driving the fluid can be written as:

$$\mathbf{f}(\mathbf{x}) = F\phi(y/l)\mathbf{e}_x, \quad (2.3)$$

where l is the longest length scale in the forcing function, here the characteristic length of the domain, and F the amplitude. The dimensionless square integrable (or smoother) shape function $\phi \in L^2[0, 1]$ satisfies homogeneous Neumann boundary conditions with zero mean:

$$\phi'(0) = \phi'(1), \quad \int_0^1 \phi(\eta) d\eta = 0. \quad (2.4)$$

The shape function is normalized by:

$$1 = \int_0^1 \phi(\eta)^2 d\eta. \quad (2.5)$$

defining an unique amplitude F for a given \mathbf{f} . For practical purposes, the dimensionless potential $\Phi \in H^1[0, 1]$, the space of functions with square-integrable first derivatives, is introduced. $\Phi' = -\phi$ and Φ satisfies homogeneous Dirichlet boundary conditions, $\Phi(0) = \Phi(1)$.

Next, we introduce a mean zero multiplier function $\psi \in H^2[0, 1]$ not orthogonal to ϕ , $\langle \phi\psi \rangle \neq 0$, and satisfying homogeneous Neumann boundary conditions $\psi'(0) = \psi'(1)$. We define, $\Psi \in H^1[0, 1]$, the derivative of the multiplier function ($\Psi = \psi'$) satisfying homogeneous Dirichlet boundary conditions $\Psi(0) = \Psi(1)$. The inner product of ϕ and ψ is equal to the inner product of Φ and Ψ , *i.e.* $\langle \Phi\Psi \rangle = \langle \phi\psi \rangle \neq 0$.

2.2. Variational problem and solution

For a steady state flow, the mean energy injected by the forcing $F\langle \phi u_x \rangle$ should be equal to the total dissipation ε :

$$\varepsilon = \nu \langle |\nabla \mathbf{u}|^2 \rangle = F \langle \phi u_x \rangle. \quad (2.6)$$

Another expression for the forcing amplitude F can be obtained by projecting the streamwise component of the Navier-Stokes equations onto the multiplier function ψ . The inner product of the Navier-Stokes equations with $\psi(y/l)\mathbf{e}_x$ is integrated by parts over the volume. Then the long-time average yields:

$$-\left\langle \frac{1}{l} \psi' u_x u_y \right\rangle = \left\langle \frac{\nu}{l^2} \psi'' u_x \right\rangle + F \langle \phi\psi \rangle. \quad (2.7)$$

Then equation 2.6, becomes:

$$\varepsilon = -\frac{\langle \phi u_x \rangle \left\langle \frac{1}{l} \psi' u_x u_y + \frac{\nu}{l^2} \psi'' u_x \right\rangle}{\langle \phi\psi \rangle}. \quad (2.8)$$

An expression for the dimensionless dissipation factor β is obtained by dividing by U^3/l :

$$\beta = \frac{\varepsilon l}{U^3} = -\frac{\langle \phi \left(\frac{u_x}{U} \right) \rangle \left\langle \psi' \left(\frac{u_x}{U} \right) \left(\frac{u_y}{U} \right) + Re^{-1} \psi'' \left(\frac{u_x}{U} \right) \right\rangle}{\langle \phi\psi \rangle} \quad (2.9)$$

Changing the velocity variables to normalized velocities $u\mathbf{e}_x + v\mathbf{e}_y + w\mathbf{e}_z = U^{-1}(u_x\mathbf{e}_x + u_y\mathbf{e}_y + u_z\mathbf{e}_z)$, so that $\langle u^2 + v^2 + w^2 \rangle = 1$, and using the potential Φ and derivative multiplier Ψ , equation 2.9 is recasted as:

$$\beta = \frac{\langle \Phi' u \rangle \langle \Psi u v + Re^{-1} \Psi' u \rangle}{\langle \Phi\Psi \rangle} \quad (2.10)$$

The upper bound β_b on the dissipation factor is obtained by maximizing the right-hand

side of 2.10 over the normalized velocity field, and then minimizing over all multiplier functions Ψ :

$$\beta \leq \min_{\Psi} \max_{\mathbf{u}} \left[\frac{\langle \Phi' u \rangle \langle \Psi u v \rangle}{\langle \Phi \Psi \rangle} + Re^{-1} \frac{\langle \Phi' u \rangle \langle \Psi' u \rangle}{\langle \Phi \Psi \rangle} \right] = \beta_b(Re), \quad (2.11)$$

for any solution of the Navier-Stokes equations. β_b depends explicitly only on the Reynolds number and on the shape ($\Phi' = -\phi$) of the applied force.

The evaluation of $\beta_b(Re)$ going beyond the scope of this paper, we refer to Doering *et al.* (2003) for that matter and just give their result:

$$\beta_b(Re) = \min_{\Psi} \frac{\langle \phi^2 \rangle^{1/2}}{\langle \Phi \Psi \rangle} \left[\frac{1}{\sqrt{27}} \sup_{y \in [0,1]} |\Psi(y)| + Re^{-1} \langle \Psi'^2 \rangle^{1/2} \right]. \quad (2.12)$$

Finally, these authors solve exactly the extremization problem for the optimal Ψ in the asymptotic case $Re \rightarrow \infty$:

$$\lim_{Re \rightarrow \infty} \sup \beta_b(Re) \leq \beta_b(\infty) = \frac{1}{\sqrt{27}} \frac{\sqrt{\langle \phi^2 \rangle}}{\langle |\Phi| \rangle} \quad (2.13)$$

The shape function being normalized (*i.e.* $\langle \phi^2 \rangle = 1$), we can simplify this bound a little further:

$$\beta_b(\infty) = \frac{1}{\sqrt{27} \langle |\Phi| \rangle} \quad (2.14)$$

3. Force-shape dependence of the dissipation factor

A non-trivial body-force-shape is tested based on the Kolmogorov forcing. A second wave number is added with different amplitudes A_k to the wave number $k = 1$ used in the traditional Kolmogorov forcing:

$$f(\mathbf{x}) = [\sin(2\pi\eta) + A_k \sin(2\pi k\eta)] \mathbf{e}_x = F\phi(\eta) \mathbf{e}_x, \quad \eta \in [0, 1], \quad k \geq 1 \quad (3.1)$$

where,

$$F = \sqrt{\frac{1 + A_k^2}{2}} \quad \text{and} \quad \phi(\eta) = \sqrt{\frac{2}{1 + A_k^2}} [\sin(2\pi\eta) + A_k \sin(2\pi k\eta)], \quad (3.2)$$

with $A_1 = 0$ and $A_k \in \Re$ for $k \geq 2$. In the following, the term representing the traditional Kolmogorov forcing in equation 3.1 will often be referred as ‘‘primary term’’ and the term of higher wave number as ‘‘secondary term’’.

We can now use 2.14 in order to evaluate the bound on β in the asymptotic case $Re \rightarrow \infty$ for the non-trivial body-force-shape define above:

$$\beta_b(\infty) = \frac{1}{\sqrt{27}} \frac{1}{\int_0^1 \left| \frac{1}{2\pi} \sqrt{\frac{2}{1 + A_k^2}} (\cos(2\pi\eta) + \frac{A_k}{k} \cos(2\pi k\eta)) \right| d\eta}. \quad (3.3)$$

The integral on the denominator of the right hand side of equation 3.3 can be rather painful to solve by hand. First, we consider the simple cases.

The case of the classical Kolmogorov forcing, $k = 1$ ($A_1 = 0$), is straightforward. Equation 3.3 becomes:

$$\beta_b(\infty) = \frac{1}{\sqrt{27}} \frac{1}{\int_0^1 \left| \frac{1}{2\pi} \sqrt{2} \cos(2\pi\eta) \right| d\eta} = \frac{\pi^2}{\sqrt{54}}. \quad (3.4)$$

This result indicates that for large enough Reynolds numbers, the dissipation factor for

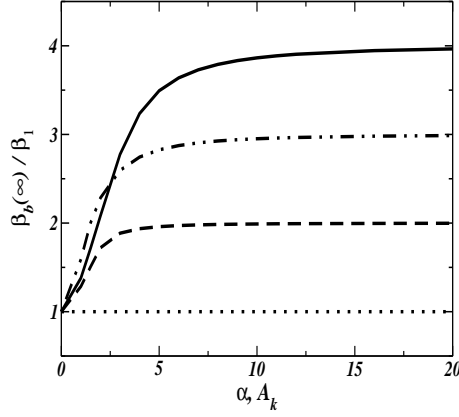


Figure 1: Solution of equation 3.3 normalized by $\beta_1 \equiv \beta_b(\infty)|_{f(x)=\alpha \sin(2\pi\eta), \alpha \in \mathfrak{R}}$ plotted as a function of the amplitude of the secondary mode forced, A_k (or α in the case of the classic Kolmogorov forcing). Dotted line: $f_x = \alpha \sin(2\pi\eta), \alpha \in \mathfrak{R}$; Dashed line: $f_x = \sin(2\pi\eta) + A_2 \sin(2 \times 2\pi\eta)$; Dash-dot-dot line: $f_x = \sin(2\pi\eta) + A_3 \sin(3 \times 2\pi\eta)$; solid line: $f_x = \sin(2\pi\eta) + A_4 \sin(4 \times 2\pi\eta)$.

the Kolmogorov forcing is bound from above by a constant value equal to $\pi^2/\sqrt{54}$. This value holds whatever is the amplitude of the Kolmogorov forcing.

Another trivial case appears when the secondary term becomes dominant (*i.e.* $A_k \gg 1$). The contribution of the primary term to the forcing function can therefore be neglected and the forcing becomes equivalent to a Kolmogorov forcing at a wave number greater than one:

$$\beta_b(\infty) = \frac{1}{\sqrt{27}} \frac{1}{\frac{1}{2\pi} \sqrt{\frac{2}{A_k^2}} \int_0^1 \left| \frac{A_k}{k} \cos(2\pi k\eta) \right| d\eta} = \frac{k\pi^2}{\sqrt{54}}. \quad (3.5)$$

The upper bound on β in the asymptotic case $Re \rightarrow \infty$ is linearly proportional to the wave number of the largely dominant term in the forcing function. It is not surprising that when a single mode is largely dominant in the force shape functional, the bound on the dissipation factor β is related to this particular mode. However, the linear increase of $\beta_b(\infty)$ as a function of the dominant wave number is not intuitive. This result implies that for a trivial force-shape, in other words a force-shape dictated by a single wave number, we could predict precisely the dissipation factor in the ideal case of an infinite Reynolds number. Each wave number forced alone is bound by a characteristic β_b when $Re \rightarrow \infty$.

To further understand the force-shape dependence of the bound on the dissipation factor behavior, a complete resolution of equation 3.3 is required. Figure 1 shows the evolution of the bound on the dissipation factor in the asymptotic case, $\beta_b(\infty)$, for a non-trivial force-shape normalized by the value of $\beta_b(\infty)$ obtained for a classic Kolmogorov forcing (*i.e.*, $\pi^2/\sqrt{54}$), as a function of the amplitude of the secondary term. In addition to the properties exposed by equations 3.4 and 3.5, this figure also shows that $\beta_b(\infty)$ is very sensitive to the change in shape of the forcing function. Indeed, as soon as a secondary term is added to the original Kolmogorov forcing, $\beta_b(\infty)$ increases in a quasi-linear fashion

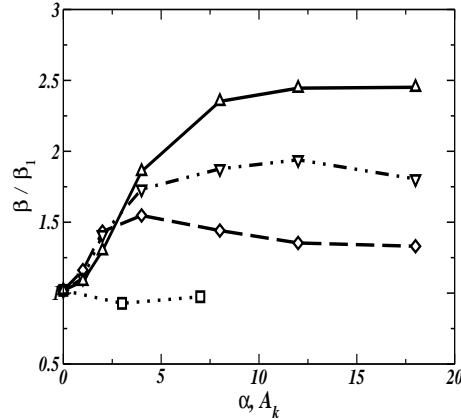


Figure 2: Dissipation factor, β , obtained by DNS and normalized by $\beta_1 \equiv \beta|_{f(\mathbf{x})=\alpha \sin(2\pi\eta), \alpha \in \mathfrak{R}}$ plotted as a function of the amplitude of the secondary mode forced, A_k (or α in the case of the classic Kolmogorov forcing). Squares, dotted line: $f = \alpha \sin(2\pi\eta)$, $\alpha = 1, 3, 7$; diamonds, dashed line: $f = \sin(2\pi\eta) + A_2 \sin(2 \times 2\pi\eta)$; down triangles, dash-dot-dot line: $f = \sin(2\pi\eta) + A_3 \sin(3 \times \pi\eta)$; up triangle, solid line: $f = \sin(2\pi\eta) + A_4 \sin(4 \times 2\pi\eta)$.

as a function of the amplitude of the secondary term. This quasi-linear increase lasts until the rate of variation of $\beta_b(\infty)$ is greater than about 80%. The increase of $\beta_b(\infty)$ then drastically slows down and plateaus. One can consider that the secondary term is largely dominant beyond this point. We can further anticipate that the characteristic features of the secondary term are the most obvious in the force profile, the contribution of the primary term being barely visible. We observe that $\beta_b(\infty)$ increases the fastest when $A_3 \sin(3 \times 2\pi\eta)$ is added to the classic Kolmogorov forcing, for small values of A_3 . We verify however that this feature is isolated and not linked to the odd wave numbers.

4. Comparison to Direct Numerical Simulations

Our Direct Numerical Simulations are performed using a fully de-aliased spectral code. The time stepping is based on a third-order Runge-Kutta algorithm for the non-linear and forcing terms. The viscous term is integrated through an analytic factor. The stability is ensured by a CFL condition. The flow is solved in a 2π in length periodic cubic box with $128 \times 128 \times 128$ grid points. The viscosity is set to $\nu = 0.015625$, large enough to ensure full spectrum resolution of the turbulent flow in our domain.

Figure 2 shows the dissipation factor β normalized by the average value of β in the case of the classic Kolmogorov forcing at different amplitudes as a function of the amplitude of the secondary term. Each symbol represents a simulation with a different force shape following the definition of equation 3.1. The symbols designing a particular secondary wave number k are linked by straight lines using the same nomenclature as in figure 1 in order to ease comparisons between the behaviors of $\beta_b(\infty)$ and β . We verify that all the simulations satisfy the convergence criterion for the Kolmogorov flow defined by Sarris *et al.* (2007). The simulations with secondary term amplitudes of $A_k = 18$ verify $k_{max}\eta > 1.2$, where k_{max} is the largest wave number of the simulation and η

the Kolmogorov length scale, slightly under the commonly used flow resolution criterion $k_{max}\eta > 1.5$.

On figure 2, we recognize the same patterns displayed on figure 1. First, β has a nearly constant value when only the wave number $k = 1$ is forced. In this particular case, a limited number of simulations was possible as for an amplitude of 7 for the forcing, the limit of resolution of our flow domain was already achieved. As regard to the force shape, we can anticipate that the value of β will remain about constant for any amplitude.

Second, in the case of a non-trivial force-shape, β increases in a nearly linear fashion as a function of A_k until the secondary term becomes dominant (A_k sufficiently large). Then, the increase in β slows down and plateaus. The analytic bound on the dissipation factor in the asymptotic case of an infinite Reynolds number predicts qualitatively the behavior of the dissipation factor at our low Reynolds number Direct Numerical Simulations. Indeed, our simulations have Taylor-scale Reynolds number, R_λ , varying between about 50 and 100. The observations made from the predicted bound on the dissipation factor when $Re \rightarrow \infty$ apply at low to moderate Re : *i*) β is very sensitive to changes in the shape of the forcing function, *ii*) β saturates at a characteristic level for a given wave number and *iii*) it seems that the level of saturation of β is linearly proportional to the wave number.

The symmetry in the qualitative results obtain from figure 1 and 2 proves that β is not only sensitive to the force-shape as observed above, but β strongly depends on it. First, when a single wave number is forced, a variation on the amplitude of the forcing function alone implies no variation on the shape (*i.e.*, the general appearance of the profile) but a linear variation of the slopes of the force-shape as a function of the amplitude. The variations of amplitude affect the total kinetic energy of the flow, so it affects U (as defined in this paper, $U \propto E^{1/2}$, where E is the total kinetic energy). The variations of the slopes affect the kinetic energy dissipation ε . In addition, according to Kolmogorov's third law, $\varepsilon \propto E^{3/2} \equiv \varepsilon \propto U^3$, for sufficiently high Reynolds numbers. Therefore, having β (about) constant is directly related to the steadiness of the force-shape in this particular case. The same reasoning applies when a given wave number is largely dominant in the force-shape. Second, when a secondary term with a small enough amplitude is added to the forcing on a single wave number, the amplitude of the new forcing function varies barely whereas the force-shape becomes significantly different (see case $A_k = 1$ on figure 4c for example). The total kinetic energy of the flow changes barely and the kinetic energy dissipation changes significantly. As a result, we observe a significant variation in β ($\beta \propto \varepsilon/E^{3/2}$). We can anticipate the same type of influence on the dissipation factor for secondary terms with large amplitude, but not large enough for the secondary term to be largely dominant.

As already observed, despite qualitative agreement, the numerical values for β are about a factor 5 below the predicted upper bound (not visible here because of the normalization of β in the figures) (Doering *et al.* 2003). Also figures 1 and 2 clearly show that the theory does not predict correctly the magnitude of the increase in β when forcing an additional wave number. The slopes in the quasi-linear part of the evolution of β are greater in figure 1 than in figure 2.

5. Mean velocity profile dependence on the force profile

Figure 3 shows the mean velocity profile $U(y)$, the Stokes flow profile $U_{stokes}(y)$, the optimal multiplier profile $\psi_m(y)$ and the corresponding forcing function $f(y) = \sin(y) + \sin(ky)$, where $k = 2, 3, 4$ respectively in *a*), *b*) and *c*). The Stokes flow is the flow associated with a lower bound on the dissipation factor β . The Stokes flow profile is

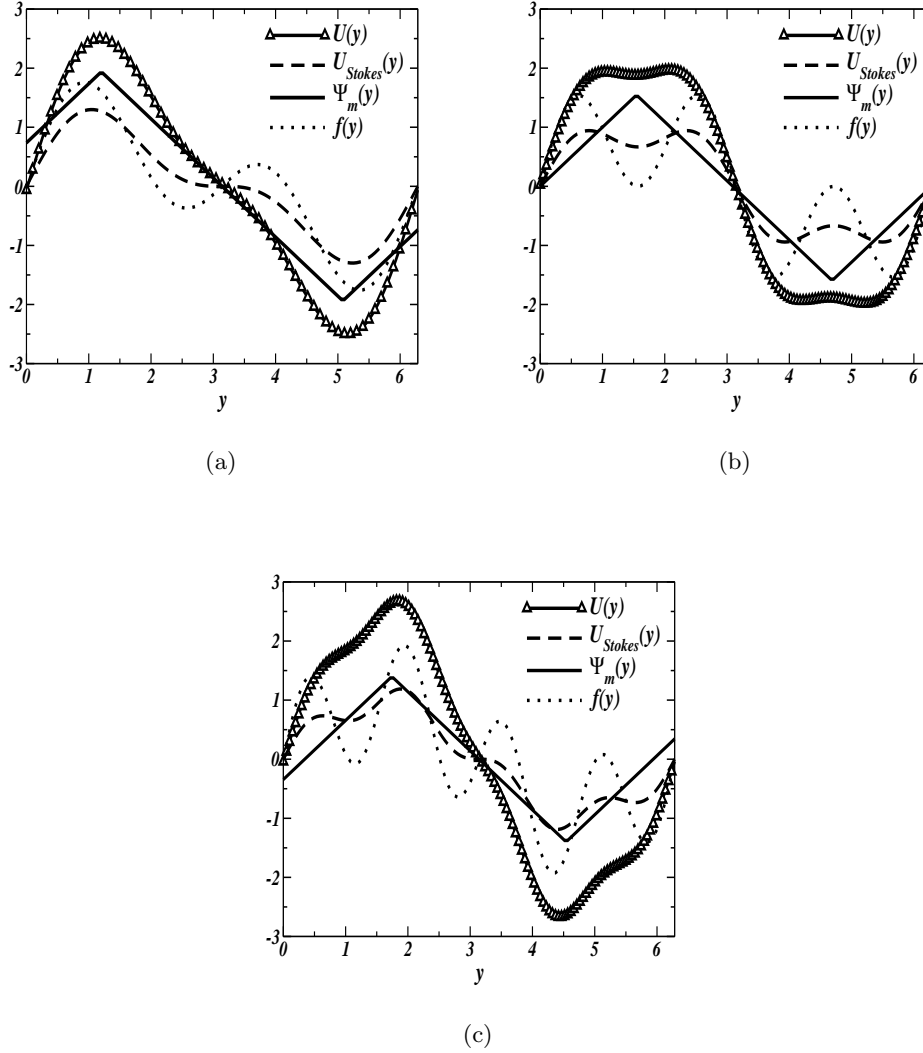


Figure 3: Mean velocity profile $U(y)$ (solid line and triangles), Stokes flow profile $U_{Stokes}(y)$ (dashed line), optimal multiplier profile $\Psi_m(y)$ (solid line) and corresponding forcing profile $f(y)$ (dotted line). a) $f(y) = \sin(y) + \sin(2y)$, b) $f(y) = \sin(y) + \sin(3y)$, c) $f(y) = \sin(y) + \sin(4y)$.

simply obtained by integrating twice the forcing function:

$$U_{Stokes}(y) = \int_0^y \left(\int_0^{y'} F \phi(y'') dy'' \right) dy' + C, \quad (5.1)$$

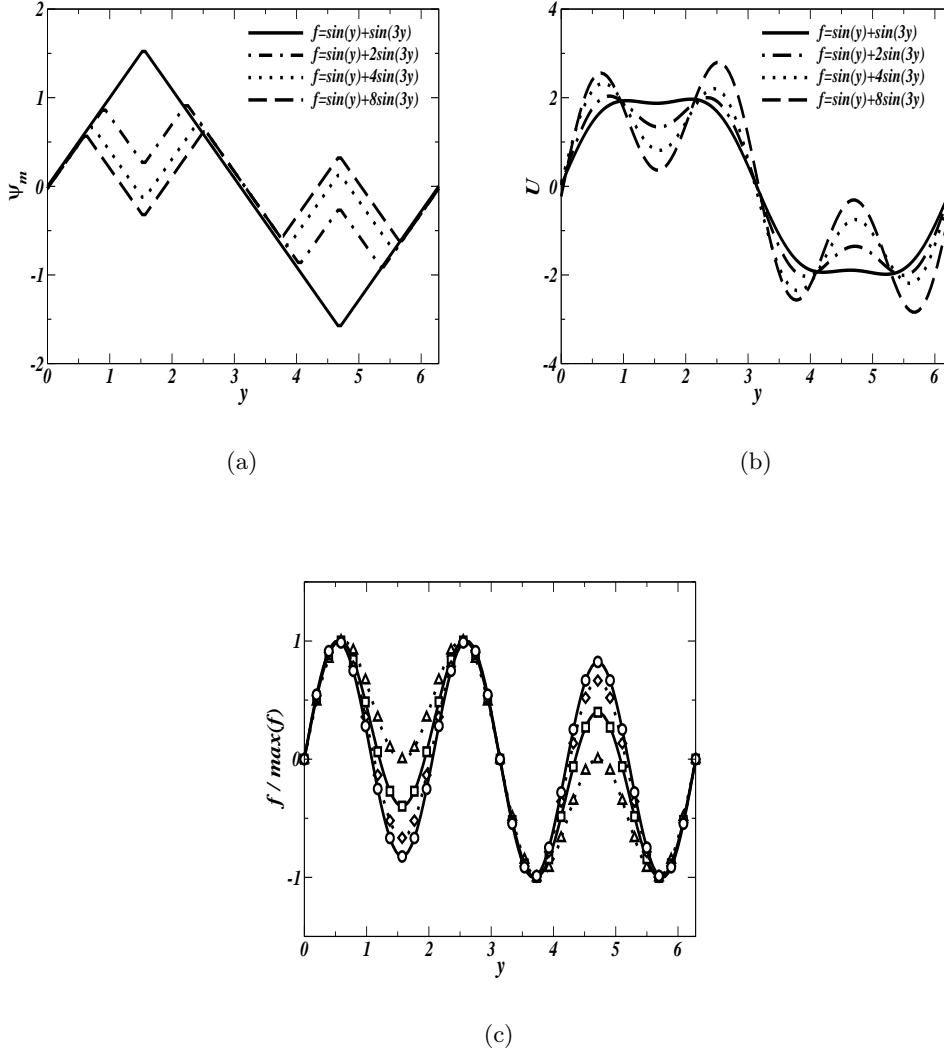


Figure 4: *a*) Optimal multiplier profile $\psi_m(y)$ for the force profile $f(y) = \sin(y) + A_k \sin(3y)$, $A_k = 1, 2, 4, 8$. *b*) Mean velocity profile $U(y)$ for the force profile $f(y) = \sin(y) + A_k \sin(3y)$, $A_k = 1, 2, 4, 8$. *c*) Force profile $f(y) = \sin(y) + A_k \sin(3y)$, $A_k = 1, 2, 4, 8$, normalized by $\max(f)$, its maximum value. Triangles on dotted line: $A_k = 1$; squares on solid line: $A_k = 2$; diamonds on dotted line: $A_k = 4$; circles on solid line: $A_k = 8$.

where C is a constant always equal to 0 in our configuration. The optimal multiplier ψ_m in the case of infinite Reynolds numbers is given by:

$$\psi_m(y) = \int_0^y \operatorname{sgn} \left(\int_0^{y'} \phi(y'') dy'' \right) dy' + C, \quad (5.2)$$

where C is a constant determined by using the zero mean condition on ϕ . We made here the hypothesis that the optimal multiplier at finite Reynolds numbers is identical to the infinite Reynolds numbers optimal multiplier.

In the cases presented on figure 3, the low wave number term in the forcing function is the dominant term. Contrary to the DNS presented by Doering *et al.* (2003), our domain is periodic in all three directions. There are no free-slip boundary conditions to constrain the velocity profiles. Thus, the key feature of these velocity profiles is that they display all the characteristic elements of the force profile. These elements appear to various extent whether we have a Stokes flow or a fully developed turbulent flow. For the velocity profiles shown in these figures, the dominant shape is clearly a sine function because of the small contribution of the secondary term. But, we see by looking at the force profiles that a well defined change in slope induces a change in slope for the velocity profiles. These changes are more obvious in Stokes profiles (figure 3) than in the turbulent flow mean velocity profiles. Indeed, in the turbulent case, a deviation in the force profile as seen on figure 3a around $y = \pi$ creates too little of a shear on a too little sub-domain compared to the combined effect of the shear on both sides of this sub-domain. Functions of high wave number provide less energetic contribution to the turbulent flow than functions of low wave number. Therefore, the weight on the secondary term of the forcing function must be greater than the weight on the primary term in order to have at least an equivalent contribution to the turbulent flow. Hence the minute contribution to the Stokes and turbulent mean velocity profiles of the secondary term in figure 3. The optimal multiplier profiles relate to the dominant term of the forcing functions. They appear to indicate only significant contributions to the force profile, here the primary term.

Figure 4 allows a broader perspective on behavior of the optimal multiplier ψ_m . It shows the optimal multiplier profile, the mean velocity profile and the normalized force profile as the amplitude on the secondary mode is increased. As mentioned above, ψ_m appears to be less sensitive than the mean velocity profile as regard to the forcing profile. Indeed, we verify that for the cases $f(y) = \sin(y)$ and $f(y) = \sin(y) + \sin(3y)$, ψ_m displays the same profile. For larger amplitudes ($A_k \geq 2$) on the secondary term, ψ_m displays a shape characteristic to the wave numbers composing the force-shape. As the amplitude on the secondary term increases, the amplitude of ψ_m decreases (figure 4a). The decrease in the amplitude of ψ_m is slower as the amplitude on the secondary term gets larger. We can relate the evolution of ψ_m to the evolution of the slopes of the features characteristic to the secondary term in the force-shape profile. In figure 4c, the local minimum at $\pi/4$ and local maximum at $3\pi/4$ are caused by the addition of the secondary term. We observe that the variation of the slopes around these points is smaller as the amplitude on the secondary term increases. We verify that this variation of slope becomes constant as the secondary term becomes largely dominant (contribution of the primary term negligible). Therefore, amplitude of the optimal multiplier remains constant when the secondary term is largely dominant. Finally, figure 4b shows that the relation between ψ_m and the mean velocity profile is unclear. For $f(y) = \sin(y) + \sin(3y)$, the optimal multiplier shows no indication of the influence of the secondary term whereas the mean velocity profile does.

6. Conclusions

To summarize, low Reynolds number Direct Numerical Simulations confirmed qualitative results predicted by the mathematical analysis at infinite Reynolds numbers. This confirms the dependence of the dissipation factor on the force-shape as predicted by the solution of the optimization problem. We can discern two major tendencies: i) when

the forcing function is mainly shaped by a single wave number, the dissipation factor is unique, its value being seemingly proportional to the dominant wave number. *ii*) β increases in a quasi-linear fashion when an additional term is added to the forcing function until this additional term becomes dominant.

Also, we observed that the mean velocity profiles display all the characteristic features of the forcing function in a 3D-periodic domain. The extent of these features are modulated as a function of the contribution of each component on the forcing function. As a consequence, in 3D-periodic domains, it should be possible to manipulate the force-shape in order to obtain a given mean velocity profile. The optimal multiplier evolution is tied to the force-shape, but its relation to the mean velocity profile remains unclear.

In this short paper, we showed that in unbound turbulence, the force-shape plays a major role in the energy dissipation rate. The optimization problem solved by Doering *et al.* (2003) captures this dependence qualitatively for any forcing function. We demonstrated that their high Reynolds numbers prediction remains valid for moderate Reynolds numbers. Improvements in the quantitative prediction of the dissipation factor remain necessary in order to be able to use the dissipation in a turbulence model.

The computational resources provided by the Vermont Advanced Computing Center, which is supported by NASA (Grant No. NNX 06AC88G), are gratefully acknowledged. We are also grateful to Professors Carati and Knaepen and all the Turbo team for providing the code.

REFERENCES

- CHILDRESS, S., KERSWELL, R.R. & GILBERT, A.D. 2001 Bounds on dissipation for Navier–Stokes flow with Kolmogorov forcing. *Physica D: Nonlinear Phenomena* **158** (1-4), 105–128.
- CONSTANTIN, P. & DOERING, C.R. 1995 Variational bounds on energy dissipation in incompressible flows. II. Channel flow. *Physical Review E* **51** (4), 3192–3198.
- DOERING, C.R. & CONSTANTIN, P. 1992 Energy dissipation in shear driven turbulence. *Physical Review Letters* **69** (11), 1648–1651.
- DOERING, C.R. & CONSTANTIN, P. 1994 Variational bounds on energy dissipation in incompressible flows: Shear flow. *Physical Review E* **49** (5), 4087–4099.
- DOERING, C.R., ECKHARDT, B. & SCHUMACHER, J. 2003 Energy dissipation in body-forced plane shear flow. *Journal of Fluid Mechanics* **494**, 275–284.
- DOERING, C.R. & FOIAS, C. 2002 Energy dissipation in body-forced turbulence. *Journal of Fluid Mechanics* **467**, 289–306.
- FRISCH, U. 1995 *Turbulence: The Legacy of AN Kolmogorov*. Cambridge University Press.
- JIMÉNEZ, J. & MOIN, P. 1991 The minimal flow unit in near-wall turbulence. *Journal of Fluid Mechanics* **225**, 213–240.
- KERSWELL, R.R. 1998 Unification of variational principles for turbulent shear flows: the background method of Doering-Constantin and the mean-fluctuation formulation of Howard-Busse. *Physica D: Nonlinear Phenomena* **121** (1-2), 175–192.
- KOLMOGOROV, A. 1941 The Local Structure of Turbulence in Incompressible Viscous Fluid for Very Large Reynolds' Numbers. *Dokl. Akad. Nauk SSSR* **30**, 301–305.
- MARCHIORO, C. 1994 Remark on the energy dissipation in shear driven turbulence. *Physica D* **74** (3-4), 395–398.
- NICODEMUS, R., GROSSMANN, S. & HOLTHAUS, M. 1998 The background flow method. Part 1. Constructive approach to bounds on energy dissipation. *Journal of Fluid Mechanics* **363**, 281–300.
- RICHARDSON, L.F. 1922 *Weather Prediction by Numerical Process*. University Press.
- SARRIS, I.E., JEANMART, H., CARATI, D. & WINCKELMANS, G. 2007 Box-size dependence and breaking of translational invariance in the velocity statistics computed from three-dimensional turbulent Kolmogorov flows. *Physics of Fluids* **19**, 095101.

- SREENIVASAN, KR 1984 On the scaling of the turbulence energy dissipation rate. *Physics of Fluids* **27**, 1048.
- SREENIVASAN, K.R. 1998 An update on the energy dissipation rate in isotropic turbulence. *Physics of Fluids* **10**, 528.
- TAYLOR, GI 1938 The Spectrum of Turbulence. *Proceedings of the Royal Society of London. Series A, Mathematical and Physical Sciences* **164** (919), 476–490.
- WANG, X. 1997 Time averaged energy dissipation rate for shear driven flows in R n. *Physica D: Nonlinear Phenomena* **99** (4), 555–563.